

Effect of SiC reinforcement particles on the grain density in a magnesium-based metal–matrix composite: Modelling and experiment

Janusz Lelito^{a,*}, Pawel L. Zak^a, Amir A. Shirzadi^{b,c}, A. Lindsay Greer^c,
Witold K. Krajewski^a, Jozef S. Suchy^a, Katharina Haberl^d, Peter Schumacher^d

^a Department of Foundry Processes Engineering, Faculty of Foundry Engineering, AGH University of Science and Technology, Reymonta 23, 30-059 Krakow, Poland

^b Materials Engineering Group (DDEM), The Open University, Walton Hall, Milton Keynes MK7 6AA, UK

^c Department of Materials Science and Metallurgy, University of Cambridge, Pembroke Street, Cambridge CB2 3QZ, UK

^d Department of Metallurgy, University of Leoben, Franz-Josef-Strasse 18, 8700 Leoben, Austria

Received 6 September 2011; received in revised form 19 January 2012; accepted 31 January 2012

Available online 3 March 2012

Abstract

The aim of this work is to develop a numerical model capable of predicting the grain density in the Mg-based matrix phase of an AZ91/SiC composite, as a function of the diameter and total mass fraction of the embedded SiC particles. Based on earlier work in a range of alloy systems, we assume an exponential relationship between the grain density and the maximum supercooling during solidification. Analysis of data from cast samples with different thicknesses, and mass fractions and particle diameters of added SiC, permits conclusions to be drawn on the role of SiC in increasing grain density. By fitting the data, an empirical nucleation law is derived that can be used in a micro–macro model. Numerical simulations based on the model can predict the grain density of magnesium alloys containing SiC particles, using the diameter and mass fraction of the particles as inputs. These predictions are compared with measured data. © 2012 Acta Materialia Inc. Published by Elsevier Ltd. All rights reserved.

Keywords: Casting; Grain refinement; Metal–matrix composites (MMCs); Modelling; Nucleation and growth

1. Introduction

The grain size of metallic materials – pure metals, alloys or metal–matrix composites (MMCs) – substantially affects their mechanical properties. In some cases, crystal nucleation (rather than, for example, dendrite break-up) during solidification is a key factor in determining the grain size, and control of nucleation can therefore be crucial in achieving desirable properties, particularly if, as for most MMCs, the grain size cannot easily be altered by any conventional post-solidification heat treatment.

Software from several sources, including commercial, can simulate the nucleation and growth of grains within a solidifying liquid and predict the microstructure of the

resultant solid phase(s) [1–6]. However, the presence of reinforcement particles (e.g. alumina or silicon carbide) in an MMC makes the modelling of the solidification more complicated [7–11]. Typically, the grain size in the metallic matrix becomes smaller as more particles are added, but the mechanisms of this refinement remain unclear. In this work a numerical model is developed, with input parameters derived by fitting measured data. Building on earlier work [12–16], the model is used to predict the grain density in an MMC with an Mg–Al–Zn matrix (AZ91 alloy) containing different amounts of SiC particles, and the effect of the diameter of SiC particles is also investigated.

It is commonly reported that for MMCs, the addition of reinforcement particles significantly affects the grain size in the metal matrix [14,17–20]. For the present work, it is relevant that Mg–Al–Zn castings show a finer grain size when reinforced with SiC particles [13,14,16,21–24]. The

* Corresponding author. Tel.: +48 12 617 4718; fax: +48 12 633 6348.
E-mail address: lelito@agh.edu.pl (J. Lelito).

resulting MMCs also show improved mechanical properties [24]. The surfaces of ceramic particles are potential sites for heterogeneous nucleation during crystallization of liquid alloys [22]. If the misfit in interatomic spacings in the interface planes of the ceramic and the nucleating phase is less than 5%, potent nucleation catalysis can be expected [25]. Cai et al. [26,27] have shown that for SiC (6H α type) and magnesium primary phase (α -Mg), the smallest misfit (2.3%) is obtained for the crystallographic orientation relationship $(10\bar{1}0)_{\text{Mg}} // (0001)_{\text{SiC}}$, suggesting possible potent nucleation for this case. The SiC particles are polycrystalline, and the optimum crystallographic surfaces are not always exposed to the liquid alloy, so that even large particles may fail to be effective nucleants. However, a larger population of SiC particles overall should give a larger population of active nucleant particles.

2. Solidification model

In the present numerical micro–macro model it is assumed that the magnesium-based liquid solidifies to an Mg–Al single phase; for simplicity, the formation of any eutectic structure is not considered. During computations for AZ91-based composites the zinc content was omitted, the metal matrix being treated as an Mg–9 Al binary alloy. The temperature field within both solid and liquid phases can be described by the Fourier–Kirchhoff equation:

$$\frac{\partial T}{\partial \tau} = a \nabla^2 T + \frac{q_V}{C_V}, \quad (1)$$

where T is the temperature (K), τ is the time (s), a is the thermal diffusivity ($\text{m}^2 \text{s}^{-1}$), q_V is the latent heat release rate (W m^{-3}) and C_V is the specific heat ($\text{J m}^{-3} \text{K}^{-1}$), taken to be the same for both phases. The latent heat release rate is defined by

$$q_V = L \frac{\partial f_S}{\partial \tau}, \quad (2)$$

where L is the latent heat of crystallization of the magnesium primary phase (J m^{-3}) and f_S is the solid fraction. The instantaneous value of f_S is calculated from the number N_i and radius R_i of the grains at each iteration step:

$$f_S = 1 - \exp\left(-\sum_{i=1}^n \frac{4\pi}{3} R_i^3 N_i\right). \quad (3)$$

To facilitate the calculation, the initial radius of all freshly nucleated grains is taken to be 1 μm . The overall growth rate of the solid phase is modelled using Eq. (4), the first part of which accounts for the growth of existing grains and the second part for the increasing number of grains:

$$\frac{\partial f_S}{\partial \tau} = (1 - f_S) \left(\sum_{i=1}^n 4\pi R_i^2 N_i \frac{\partial R_i}{\partial \tau} + \frac{4}{3} \pi R_{n+1}^3 \frac{\partial N_V}{\partial \tau} \right), \quad (4)$$

where N_V is the volumetric grain density (m^{-3}). The solidification model assumes spherical growth of the primary

phase. The growth rate is controlled by solute diffusion, in this case by the diffusion of Al in the Mg-based liquid in front of the moving solid–liquid interface. Eqs. (5) and (6) are based on Fick’s second law in a spherical coordinate system [28,29] and give the transient concentrations of aluminium in the solid and liquid phases, respectively:

$$\text{solid phase (primary } \alpha): \frac{\partial C_\alpha}{\partial \tau} = D_\alpha \left(\frac{\partial^2 C_\alpha}{\partial r^2} + \frac{2}{r} \frac{\partial C_\alpha}{\partial r} \right) + \frac{r}{R} \frac{\partial C_\alpha}{\partial r} \frac{\partial R}{\partial \tau}, \quad (5)$$

$$\text{liquid phase: } \frac{\partial C_L}{\partial \tau} = D_L \left(\frac{\partial^2 C_L}{\partial r^2} + \frac{2}{r} \frac{\partial C_L}{\partial r} \right) + \frac{R_0 - r}{R_0 - R} \frac{\partial C_L}{\partial r} \frac{\partial R}{\partial \tau}, \quad (6)$$

where C_L and C_α are the concentrations of Al in liquid and solid (wt.%), r is the distance from the grain centre, R is the radius of a spherical grain and R_0 the maximum radius of a spherical grain if the remaining liquid solidifies to one single grain. Using Eqs. (5) and (6) and applying the mass balance of the partitioning solute (i.e. Al), the growth rate of a solid grain can be calculated:

$$(C_L^0 - C_\alpha^0) \frac{\partial R}{\partial \tau} = D_\alpha \frac{\partial C_\alpha}{\partial r} \Big|_{r=R^-} - D_L \frac{\partial C_L}{\partial r} \Big|_{r=R^+}, \quad (7)$$

where D_α , D_L and C_α^0 , C_L^0 are respectively the diffusivities and the equilibrium concentrations of aluminium in solid and liquid phases in the Mg–Al phase diagram. The boundary conditions are:

- at the solid–liquid interface: $C = C_\alpha^0$, $r = R^-$, on the grain side; and $C = C_L^0$, $r = R^+$, on the liquid side,
- in the centre of a grain: $\frac{\partial C_\alpha}{\partial r} \Big|_{r=0} = 0$, and
- in the liquid far from a grain: $\frac{\partial C_L}{\partial r} \Big|_{r=R_0} = 0$.

3. Experimental methods

The magnesium alloy AZ91, with about 9 Al, 0.6 Zn, 0.2 Mn, 0.03 Si, 0.002 Fe, 0.003 Cu and 0.001 Ni (all wt.%), was selected as the matrix for this work. The samples contained 0, 0.1, 0.5, 1, 2 or 3.5 wt.% sharp SiC particles (from Polmineral) with nominal arithmetic mean diameters of 10, 40 or 76 μm . About 1.4 kg of the AZ91 alloy was melted in a steel crucible, using an electric resistance furnace filled with SF₆/CO₂ shielding gas, and kept at 700 °C for 1 h before adding the SiC particles pre-heated to 450 °C. The melt was mechanically stirred for 2 min to ensure a uniform distribution of the SiC particles (similar to the procedure of Luo [21]), and then cast into a resin-hardened sand mould with cores and gating system as shown in Fig. 1. The mould was designed to produce four 100 × 100 mm² plates with a thickness of 10, 15, 20 or 30 mm, giving a range of cooling rates. Analysis was based on the mean of values determined from three experiments performed under the same conditions.

To obtain the cooling curves of the samples, a four-channel data-logging system with an acquisition rate of 5 readings s⁻¹ was used to record the change in temperature vs. time from a K-type thermocouple positioned in the centre of each plate (~50 mm above the base plate shown in Fig. 1). A num-

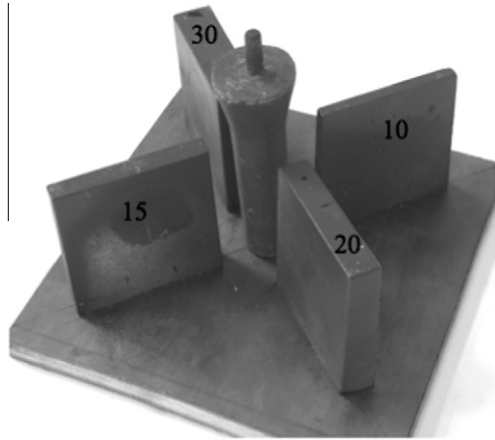


Fig. 1. Gating system and wooden model used for casting four $100 \times 100 \text{ mm}^2$ composite plates with thicknesses of 10, 15, 20 or 30 mm.

ber of cuboid samples with a cross-section of $35 \times 35 \text{ mm}^2$ and height of 45 mm were also cast from composites containing different diameters of SiC particles. The thermocouple was located in the centre of the cuboid crucible.

Metallographic specimens, taken from the cast plates at a distance of 3 mm from the hot junction of the embedded thermocouples, were ground and polished using conventional preparation methods, and then etched at room temperature. Some specimens were selected for detailed metallographic study (to identify the components in the microstructure; these specimens were etched for 5 s in a solution of 5 ml ethanoic acid in 80 ml H_2O). The specimens selected for grain density measurement were etched for ~ 90 s in a solution containing 50 ml distilled water, 150 ml ethanol and 1 ml ethanoic acid [13,14,30,31]. The etched specimens were examined in white polarized light (using crossed polars and a first-order retardation plate). The planar grain density was measured using the image-analysis software NIS-Elements 3.0. The planar grain density N_A was obtained from a population of 100 grains, and the volumetric density N_V is calculated from N_A using [32]

$$N_V = \frac{2}{\pi} N_A \left(\frac{1}{d} \right)_{\text{mean}}, \quad (8)$$

where $(1/d)_{\text{mean}}$ is the mean value of the inverse diameters of all observed grain intercepts.

The phases present in the castings were identified using X-ray diffractometry (Bragg–Brentano geometry, Bruker diffractometer, with Cu K_α radiation).

4. Grain density and maximum supercooling

The supercooling at which a nucleant particle becomes active is that at which there can be free growth of the nucleated grain from the particle. Greer et al. suggested that this critical supercooling is inversely proportional to the particle diameter [33]. Thus, on cooling an alloy containing nucleant particles, nucleation occurs first on the largest particles. The number of nucleation events as a function

of supercooling then depends on the particle diameter distribution. For a commercial grain refiner used in aluminium alloys, Greer et al. [33] made direct measurements of the diameter distribution and reported that at the largest diameters relevant for grain nucleation, the distribution is exponential: the population larger than a given diameter d is proportional to $\exp(-d/\delta)$, where δ is a length characterizing the width of the distribution. Fraš et al. [34] analysed the nucleation of eutectic colonies in cast iron, and arrived at the same form of diameter distribution of nucleant particles.

Other forms of diameter distribution have been considered. Indeed, Fraš et al. [34] noted that the diameter of nucleant particles might follow a Weibull distribution, but found that their data were best fitted with a Weibull modulus of one, which is a simple exponential distribution. Other studies [35,36], modelling the effect of nucleant diameter distribution to guide the design of better grain refiners for aluminium alloys, have considered Gaussian and log-normal diameter distributions. All of these, however, closely resemble an exponential distribution at the largest particle diameters (which are the only ones likely to play a role in grain nucleation [33]).

As expressed by Fraš et al. [34], the inverse relationship of nucleation supercooling and particle diameter, for an exponential diameter distribution, directly gives a relation between the number of grains per unit volume (the volumetric grain density, N_V) and the maximum supercooling of the melt ΔT_{max} , in the form

$$N_V = \lambda \exp\left(-\frac{b}{\Delta T_{\text{max}}}\right), \quad (9)$$

where λ (m^{-3}) and b (K) are parameters to be estimated by fitting measured data. The model of Fraš et al. [34] assumes that grain nucleation occurs on a particle of diameter d when $d = 2r^* \sin\theta$, where r^* is the critical radius for nucleation of solid in the liquid and θ is the contact angle of the solid nucleus on the particle substrate. As shown by Greer et al. [33], the limited diameter of the particles invalidates this approach: the contact angle becomes irrelevant and nucleation occurs when $d = 2r^*$. Eq. (9) remains fully valid, however: the interpretation of the fitting parameter b is just altered by the removal of the $\sin\theta$ factor.

Based on these experimental studies of systems as diverse as commercial-purity aluminium alloys and cast irons, and on reasonable mathematical fitting of the diameter distribution of the largest nucleant particles, it seems that Eq. (9) should have a general validity when nucleation of grains is on a well-defined set of particles. We take this equation as the basis for our analysis in the present work.

5. Results and discussion

5.1. As-cast microstructure

The solidification of the matrix of AZ91 is expected to begin with the formation of primary α -Mg, with aluminium

and zinc being rejected into the remaining liquid. When the liquid is sufficiently concentrated in these solutes, the secondary phase $\beta\text{-Mg}_{17}(\text{Al}, \text{Zn})_{12}$ forms and the remaining liquid solidifies as a eutectic mixture of the α and β phases. Optical metallography and scanning electron microscopy (SEM) with energy-dispersive X-ray analysis (EDX) of the as-solidified microstructure are consistent with this sequence. Magnesium-rich regions, interpreted to be primary $\alpha\text{-Mg}$ grains, show dendritic microsegregation with some evidence for sixfold dendrites. Between these grains, EDX line-scans and compositional mapping show regions with composition consistent with $\beta\text{-Mg}_{17}(\text{Al}, \text{Zn})_{12}$ phase, and regions of $\alpha\text{-}\beta$ eutectic.

Fig. 2 shows X-ray diffractograms for AZ91 and for an AZ91/SiC_p composite with 5wt.% of SiC particles. In both cases, the primary $\alpha\text{-Mg}$ phase dominates, and the β -phase $\text{Mg}_{17}(\text{Al}, \text{Zn})_{12}$ formed on eutectic solidification is also detected. In the composite there is the additional phase Mg_2Si , as was also observed in earlier work [37]. The carbides Al_4C_3 [37] and Al_2MgC_2 [38] may form in magnesium-based alloys. These carbides are difficult to detect on etched surfaces or even in TEM specimens, as they react with water even at room temperature. On the other hand, X-ray diffraction data come from a significant depth (up to a few micrometres) in the sample and so may avoid problems of carbides reacting with water at the surface. The XRD studies (Fig. 2) of the as-cast composites in the present work do not show any evidence for carbides.

The microstructural feature of most direct relevance in the present work is the distribution of SiC particles. This is seen most readily in optical metallography (Fig. 3). The etched samples, under polarized light, show the metallic regions of predominant α and β phases in a range of colours, depending on composition and crystallographic orientation. The SiC particles show up as white or grey. Fig. 3a shows that most SiC particles have been pushed ahead of the growing solid grains, ending up at the grain

boundaries. A few SiC particles appear to have been trapped (entrained) within grains, presumably between dendrite side-arms. In still fewer cases (Fig. 3b) large SiC particles are observed near to grain centres, suggesting that they were nucleation sites for the grains.

The predominance of SiC particles at the grain boundaries of the AZ91 matrix phase has been observed by others [21,22,24]. Such a distribution is expected from the known inefficiency of nucleation on added particles. Even when a given ceramic phase is a potent nucleant for freezing of an alloy, most of the particles are not active as nucleants [33]. The particles that are inactive are those that require larger supercoolings for nucleation; according to the free-growth model, these are the smaller particles. As briefly reviewed by Rauber et al. [24], it is usual in the solidification of particle-reinforced MMCs that particles that do not nucleate grains are pushed into interdendritic areas, ending up aggregated on grain boundaries.

5.2. Grain-density measurements

As noted earlier, in the AZ91 alloy the total mass fraction and diameter of added SiC particles are expected to affect the grain density. The present analysis is based on Eq. (9), which is modified to take account of these effects: effect of SiC mass fraction mf_{SiC} :

$$N_V(\Delta T_{\max}, mf_{\text{SiC}}) = \lambda(mf_{\text{SiC}}) \exp\left(-\frac{b(mf_{\text{SiC}})}{\Delta T_{\max}}\right),$$

effect of SiC particle diameter d_{SiC} :

$$N_V(\Delta T_{\max}, d_{\text{SiC}}) = \lambda(d_{\text{SiC}}) \exp\left(-\frac{b(d_{\text{SiC}})}{\Delta T_{\max}}\right).$$

In this approach, λ and b in Eq. (9) are functions of the mass fraction and diameter of SiC particles. The maximum supercooling can be found from thermal analysis. It is

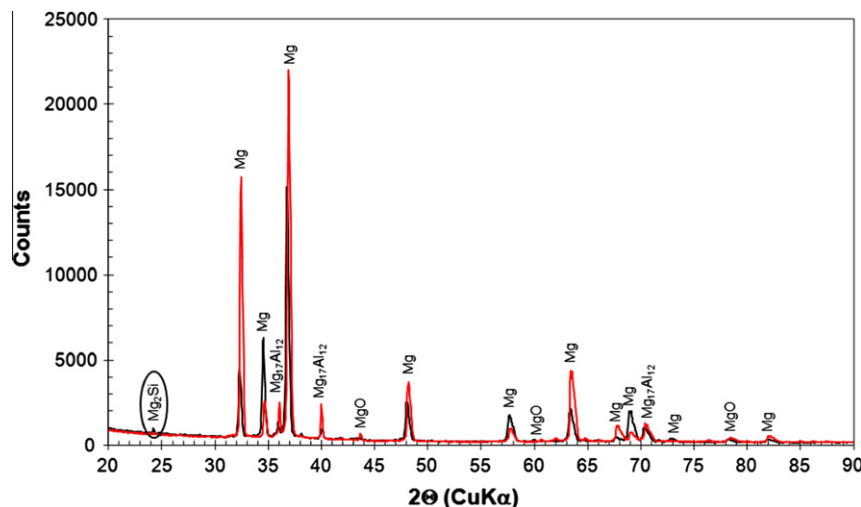


Fig. 2. X-ray diffraction traces of AZ91 alloy (red line) and composite reinforced with 5wt.% SiC (black line). The peaks have been identified, and show the same phases in the two cases, apart from the presence of Mg_2Si (circled) only in the composite.

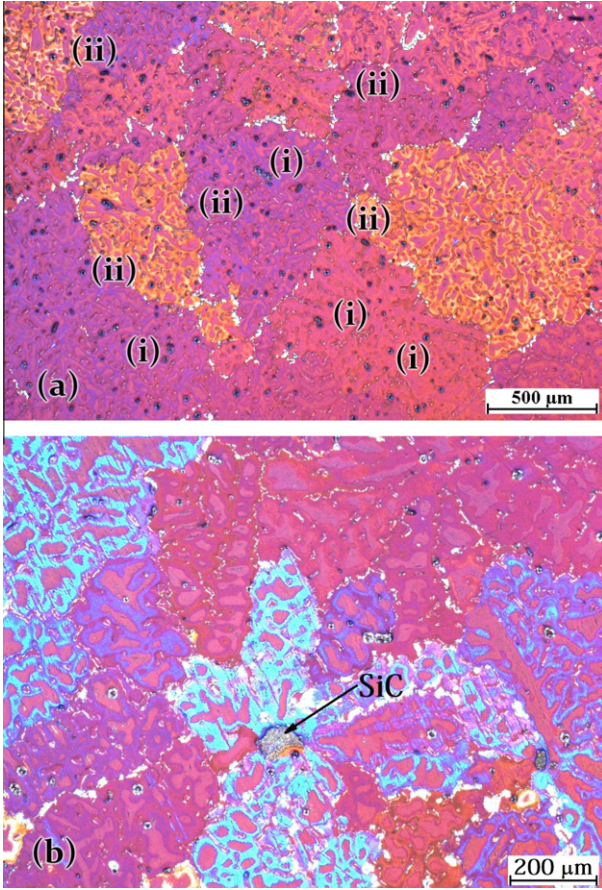


Fig. 3. Optical micrographs of the microstructure of an AZ91/SiC_p composite with 1wt.% of SiC particles (which appear white or grey): (a) overall grain structure, where the SiC particles are most evident at grain boundaries (i), but can also be found trapped within grains (ii); (b) a close-up of a large SiC particle which could be the nucleation site for this α -Mg grain.

defined as the difference between the liquidus temperature and the temperature at the onset of recalescence (Fig. 4). The tabulated equilibrium liquidus temperature for AZ91 alloy is 595 °C [39], but this value does not reflect the variability in actual composition and non-equilibrium solidification conditions. We therefore take the freezing onset, i.e. the measured nucleation temperature T_N , as the best estimate of the liquidus temperature, justifying this from the free-growth model [33]: given the largest SiC particle diameters (up to 100 μm by direct observation), the onset of freezing should occur at very small supercooling.

The change in nucleation temperature with SiC mass fraction can be estimated from the data (Fig. 5) obtained by analysing the cooling curves of one alloy matrix and five composites with 0.1, 0.5, 1, 2 or 3.5wt.% SiC using the method described by Kurz and Fisher [40]. As shown by the curve in Fig. 5, there is indeed an exponential relation between the mass fraction of SiC and nucleation temperature, as in

$$T_N(mf_{\text{SiC}}) = 881 - 5.9 \exp(-91.9mf_{\text{SiC}}). \quad (12)$$

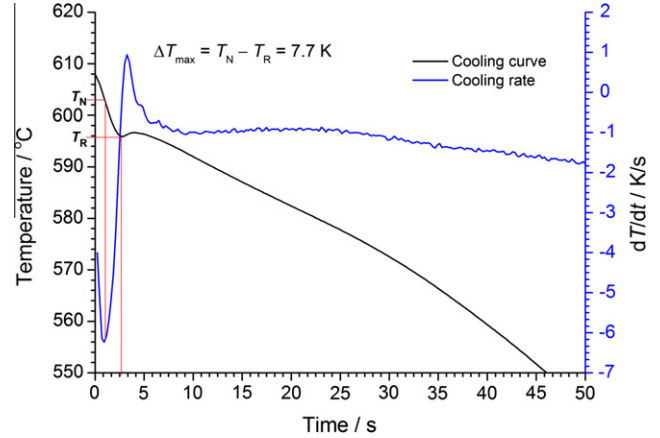


Fig. 4. Method (due to Kurz and Fisher [40]) of approximating the nucleation temperature T_N , the recalescence temperature T_R and the maximum supercooling ΔT_{max} .

Eq. (12) was then used as an input for further analysis. The parameters (λ and b) were estimated by fitting Eq. (9) to the values of grain density N_V and the maximum supercooling (ΔT_{max}) was measured for the four plate thicknesses, Table 1. Since the fitting parameters depend on the SiC particle diameter, the above calculation had to be performed for each particular case individually (i.e. for three different mean SiC particle diameters of 10, 40 or 76 μm), Table 2. With the parameter values obtained by fitting, the equations describing N_V as a function of ΔT_{max} are:

$$10 \mu\text{m SiC} : N_V(\Delta T_{\text{max}}) = 1.7 \times 10^{14} \exp\left(-\frac{43.21}{\Delta T_{\text{max}}}\right), \quad (13)$$

$$40 \mu\text{m SiC} : N_V(\Delta T_{\text{max}}) = 3.9 \times 10^{15} \times \exp\left(-\frac{93.83}{\Delta T_{\text{max}}}\right), \quad (14)$$

$$76 \mu\text{m SiC} : N_V(\Delta T_{\text{max}}) = 9.4 \times 10^{16} \times \exp\left(-\frac{135.09}{\Delta T_{\text{max}}}\right). \quad (15)$$

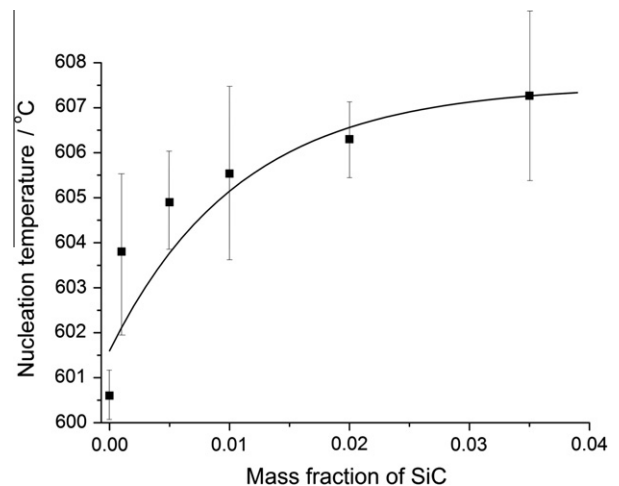


Fig. 5. Nucleation temperature T_N as a function of SiC mass fraction. The curve has been fitted to the six measured data points, each based on three measurements.

Table 1

Measurements of maximum supercooling and grain density for AZ91-based composites reinforced with different mass fractions of SiC particles, all of mean diameter 45 μm.

Plate thickness (mm)	0wt.% SiC		1wt.% SiC		2wt.% SiC		3wt.% SiC		4wt.% SiC	
	ΔT_{\max} (K)	$N_V (10^{10}) (m^{-3})$								
10	N/A	N/A	8.3	15	14.8	17	16.6	22	16.4	28
15	6.6	1.9	7.7	12	14.0	13	15.6	15	15.8	21
20	4.5	0.27	6.9	7.9	13.6	11	15.0	12	15.6	19
30	4.3	0.21	6.4	4.4	12.6	5.7	14.8	10	14.5	12

Table 2

Measurements of maximum supercooling and grain density for AZ91-based composites reinforced by SiC particles of different mean diameters. Plate thickness 35 mm.

SiC content (wt.%)	Mean particle diameter (μm)					
	10		40		76	
	ΔT_{\max} (K)	$N_V (10^{10}) (m^{-3})$	ΔT_{\max} (K)	$N_V (10^{10}) (m^{-3})$	ΔT_{\max} (K)	$N_V (10^{10}) (m^{-3})$
0	5.5	0.38	5.5	0.38	5.5	0.38
0.1	5.8	6	5.8	1	6.2	0.92
0.5	6.3	12	6.3	1.4	7.8	1.2
1	6.5	38	7.1	8.7	8.6	1.5
2	8.7	110	9.1	12	9.8	9.6
3.5	9.5	180	10.6	56	11.2	54

Combining Eqs. (13)–(15), a more general expression is derived, giving the grain density as a function of the SiC particle diameter as well as the supercooling:

$$N_V(\Delta T_{\max}, d_{SiC}) = 1.132 \times 10^{14} \times \exp\left(8.85 \times 10^4 d_{SiC} - \frac{32.6 + 1.4 \times 10^6 d_{SiC}}{\Delta T_{\max}}\right). \quad (16)$$

The correlation coefficients of all the above curve fittings are at least 0.932.

According to Eq. (9), and consistent with the free-growth model [33], the parameter *b* should be inversely proportional to substrate diameter, but this is not the trend in Eqs. (13)–(15) where *b* increases with particle diameter. While the effects of size can be complex [7], for large substrates the behaviour should be simple: for a given mass fraction of substrate particles, their population should be inversely proportional to the cube of their diameter, and the parameter λ should show the same dependence on diameter. This is again in contrast to the trend in Eqs. (13)–(15) where λ increases with particle diameter. While the correlations show that the addition of SiC particles has strong effects on the nucleation parameters λ and *b*, it is very clear that the SiC particles themselves do not have a one-to-one correspondence with the nucleant substrates for the primary-phase grains. This is not surprising, given that the SiC particles are much larger than typical inoculant particles associated with single nucleation events [33].

Adopting a similar approach, the effect of mass fraction of SiC on N_V can be calculated once the fitting parameters are determined:

$$0 \text{ wt.\% SiC } N_V = 1.184 \times 10^{12} \exp\left(-\frac{27.35}{\Delta T_{\max}}\right), \quad (17)$$

$$1 \text{ wt.\% SiC } N_V = 5.778 \times 10^{12} \exp\left(-\frac{29.95}{\Delta T_{\max}}\right), \quad (18)$$

$$2 \text{ wt.\% SiC } N_V = 5.815 \times 10^{12} \exp\left(-\frac{85.90}{\Delta T_{\max}}\right), \quad (19)$$

$$3 \text{ wt.\% SiC } N_V = 1071 \times 10^{11} \exp\left(-\frac{102.26}{\Delta T_{\max}}\right), \quad (20)$$

$$4 \text{ wt.\% SiC } N_V = 1.619 \times 10^{14} \exp\left(-\frac{104.85}{\Delta T_{\max}}\right). \quad (21)$$

The correlation coefficients of all above curve fittings are at least 0.989. The SiC particle diameter in these calculations is 45 μm. In the model of Fraš et al. [34], λ is the number of potential nucleant sites. The nucleant substrates are not individual SiC particles, but they might be sites on the particle surfaces. In that case, for a given particle diameter, λ should be proportional to the mass fraction of SiC. It is known that for higher additions of nucleant substrates, the nucleation becomes less efficient (a smaller fraction of the substrates actually initiate grains) [33]. In that case, the fitting procedure might lead to the effective value of λ rising less than proportionally with the mass fraction. In fact, however, Eqs. (17)–(21) show λ rising more than proportionally with mass fraction. This strongly suggests that the effect of the SiC particles in refining the grain size in the matrix phase cannot be attributed only to enhanced nucleation. There must be other effects such as restriction of grain growth arising from the pushing of particles. Particles being pushed could, for example, impede solute

redistribution at the solid–liquid interface. As a possible contribution to grain refinement, growth restriction was noted by Luo [21,22], but without any quantification of its significance.

Combining Eqs. (17)–(21), a more general expression is derived giving the grain density as a function of the mass fraction of SiC:

$$N_V(\Delta T_{\max}, m_{\text{SiC}}) = 1.42 \times 10^{13} \times \exp\left(61.9m_{\text{SiC}} - \frac{36.25 \exp(29.3m_{\text{SiC}})}{\Delta T_{\max}}\right), \quad (22)$$

where the correlation coefficient of the curve fitting is 0.866. Finally all the results were combined to obtain a general equation that yields the grain density of the matrix phase in the composite as a function of the mass fraction and particle diameter of SiC:

$$N_V(m_{\text{SiC}}, d_{\text{SiC}}, \Delta T_{\max}) = 9 \times 10^{13} \times \exp\left(61.9m_{\text{SiC}} - 4.1 \times 10^4 d_{\text{SiC}} - \frac{19.2 + 8.3 \times 10^5 d_{\text{SiC}} + 18.1 \exp(29.3m_{\text{SiC}})}{\Delta T_{\max}}\right), \quad (23)$$

where the correlation coefficient is 0.856. When a simple nucleation mechanism dominates, it is possible to derive the nucleation law linking N_V and ΔT_{\max} directly from the shape of the particle diameter distribution [33].

5.3. Numerical simulation

As noted above, the complex variation of grain density with arithmetic mean particle diameter and mass fraction of SiC precludes any simple nucleation analysis. In that case, there is no option but to derive an empirical nucleation law, as given in Eq. (23). The adjustable parameters in the expression are obtained by a statistical fitting to all of the experimental results. We now test whether the application of this empirical law in a numerical simulation can give quantitatively useful predictions.

Based on the model explained above, a computer program in C++ language was written to simulate the nucleation and growth of Mg–Al primary phase in the composite. As noted earlier, the eutectic reaction that takes place during non-equilibrium solidification of this alloy was ignored. As in the analyses of Maxwell and Hellawell and Greer et al. [33,41], the liquid is taken to be isothermal. Hunt [42] has recently confirmed that this is a reasonable approximation for the early stages of solidification after pouring. The temperature differences across the computational

volume are certainly small enough for a spatially uniform temperature to be assumed. The computations are performed for a single volume element. The input data in the simulation are:

- diffusion coefficients of aluminium [7]: $D_\alpha = 2.7 \times 10^{-10}$, $D_L = 2.7 \times 10^{-8} \text{ m}^2 \text{ s}^{-1}$;
- nucleation temperature calculated from Eq. (12);
- the initial temperature of the liquid is taken to be 700 °C, well above the liquidus temperature;
- $\frac{L}{C_V} = 267.86 \text{ K}$ [43];
- imposed cooling rate, $\Phi = a\nabla^2 T$, depends on temperature and mould material, and is taken to be:

$$\Phi(T) = \begin{cases} -40 & \text{for } T > 625 \text{ }^\circ\text{C} \\ \frac{200}{T-630} & \text{for } 625 \text{ }^\circ\text{C} \geq T > 620 \text{ }^\circ\text{C} \\ \frac{5T-2900}{T-630} & \text{for } 620 \text{ }^\circ\text{C} \geq T > 600 \text{ }^\circ\text{C} \\ \frac{100}{T-630} & \text{for } T \leq 600 \text{ }^\circ\text{C} . \end{cases} \quad (24)$$

Four series of simulations with SiC contents of 0.1, 2, 3 or 5wt.% were performed, using a constant arithmetic mean particle diameter of 45 μm and based on Eq. (23). This is derived from Eq. (9), which relates the final number of nucleation events per unit volume (N_V) to the maximum supercooling (ΔT_{\max}). However the same exponential form serves to relate the number of nucleation events at any instant to the supercooling at that instant. Thus ΔT_{\max} in Eq. (23) is simply replaced by the instantaneous supercooling ΔT , calculated using

$$\Delta T(\tau) = T_N - T(\tau). \quad (25)$$

Once the recalescence occurs, the model assumes no more grain nucleation. This feature of the model makes it possible to predict the grain density after complete solidification of the composite. To verify the outcome of the simulation, a number of samples were cast and their grain densities were measured. The calculated and measured grain densities are given in Table 3. Fig. 6 shows the calculated and measured cooling curves of the alloys studied in this work.

Given the assumptions made in this model and associated limitations, the predicted grain densities are reasonably close to the measured values. A key point is that the predicted and measured grain densities follow very similar trends. It is known that ceramic particles can significantly influence the thermophysical parameters of an MMC [44]. For simplicity such effects were ignored in the present simulations, but they will be considered in future work.

Table 3
Measured and calculated grain densities.

Mass fraction of SiC particles	0.1wt.%	2wt.%	3wt.%	5wt.%
$N_V (10^{11}) (\text{m}^{-3})$ (from simulation)	0.88	1.8	1.9	1.9
$N_V (10^{11}) (\text{m}^{-3})$ (from experiment)	0.95 ± 0.33	1.2 ± 0.4	1.3 ± 0.4	1.4 ± 0.3

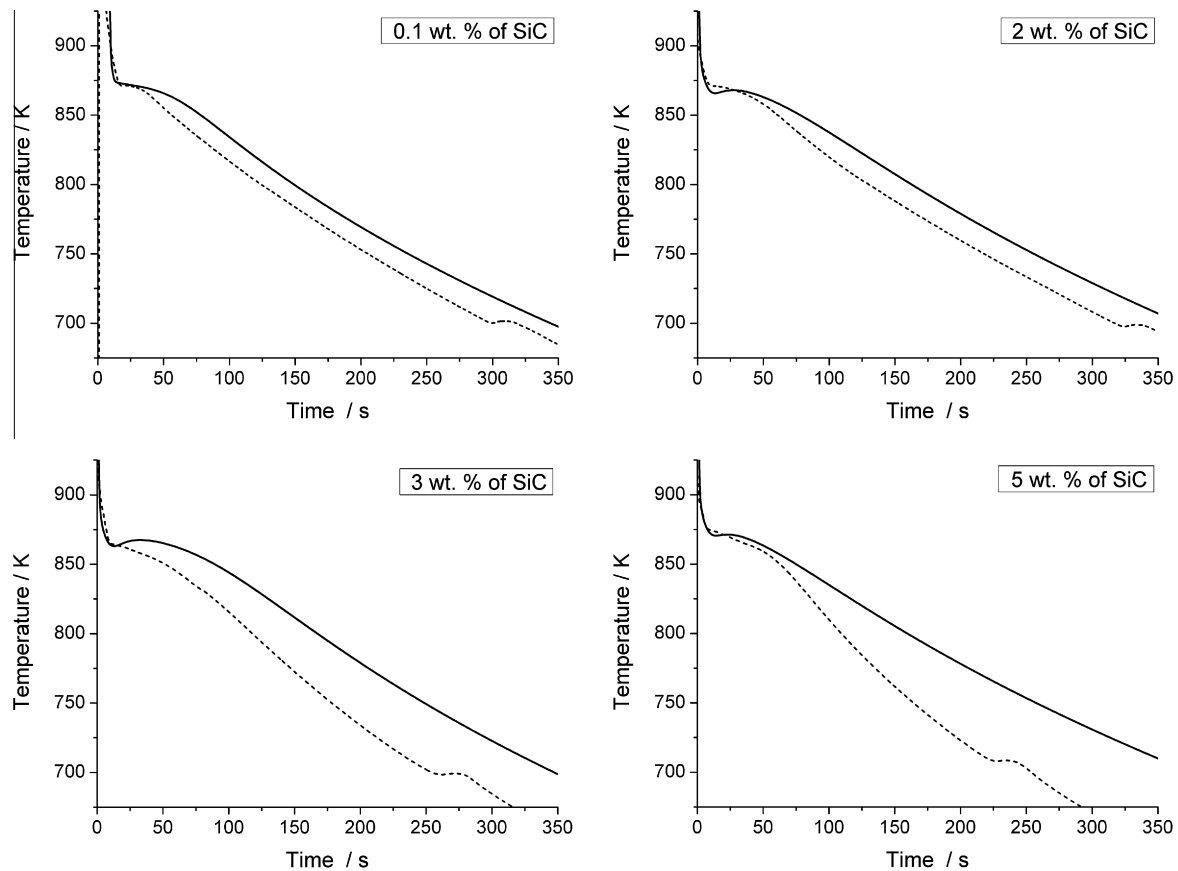


Fig. 6. Calculated (solid line) and experimental (dashed line) cooling curves for Mg–SiC composites with different SiC contents. The eutectic reaction revealed by the thermal arrest at ~ 700 K on the experimental cooling curve was not taken into consideration in the modelling.

6. Conclusions

The grain density N_V of the Mg-based matrix phase in cast AZ91/SiC composites increases markedly as the mass fraction of added SiC particles is increased, and as the particle diameter is decreased for a given mass fraction. Cooling curves were measured for plates of different thicknesses cast from alloys with different mass fractions and particles diameters of SiC. The maximum supercoolings, ΔT_{\max} , derived from the cooling curves, when related to the corresponding values of N_V , show that there is not a one-to-one correspondence between the SiC particles themselves and the nucleant substrates. In addition to possible nucleation catalysis, the addition of SiC particles may influence the grain density by effects such as growth restriction. It was therefore not possible to derive a nucleation law from fundamental mechanisms, but it was possible to calculate an empirical law by fitting the data on N_V and ΔT_{\max} . This empirical nucleation law was used in a numerical simulation based on a micro–macro model including the effects of heat and mass transfer at the solid–liquid interface. The simulation is capable of giving quantitatively acceptable predictions of cooling curves, and matrix grain densities in cast AZ91/SiC composites as a function of heat-extraction rates, and mass fraction and particle diameter of SiC.

Acknowledgements

The authors acknowledge financial support from the European Union under Marie Curie Transfer of Knowledge Grant No. MTKD-CT-2006-042468 (AGH No. 27.27.170.304).

References

- [1] Stefanescu DM, Upadhyaya G, Bandyopadhyay D. Metall Trans A 1990;21A:997.
- [2] Stefanescu DM. In: Pivonka TS, Voller V, Katgerman L, editors. Modeling of casting, welding and advanced solidification processes VI. Warrendale, PA: TMS; 1993. p. 3.
- [3] Liu J, Elliott R. J Cryst Growth 1998;191:261.
- [4] Rappaz M, Gandin CA. Acta Metall Mater 1993;41:345.
- [5] Kapturkiewicz W, Fraś E, Burbelko AA. Arch Metall Mater 2009;54:369.
- [6] Gurgul D, Burbelko AA. Arch Metall Mater 2010;55:53.
- [7] Günther R, Hartig Ch, Bormann R. Acta Mater 2006;54:5591.
- [8] Lelito J, Suchy J, Żak P, Krajewski W, Krawiec H, Greer AL, et al. Krawiec H. In: Świątkowski K, editor. Polish metallurgy 2006–2010 in time of the worldwide economic crisis. Warsaw: Comm of Metallurgy of the Polish Acad Sci; 2010. p. 123.
- [9] Cholewa M. J Mater Proc Technol 2005;164–164:1175.
- [10] Jagadeesh SK, Ramesh CS, Mallikarjuna JM, Keshavmurthy R. J Mater Proc Technol 2010;210:618.
- [11] Cetin A, Kalkanli A. J Mater Proc Technol 2009;209:4795.
- [12] Lelito J, Żak P, Suchy JS. Arch Metall Mater 2009;54:347.

- [13] Lelito J, Żak P, Suchy JS, Krajewski W, Greer AL, Darlak P. *China Foundry* 2011;8(1):101.
- [14] Gracz B, Lelito J, Żak P, Krajewski WK, Suchy JS, Szucki M. *Metall Foundry Eng* 2010;36:123.
- [15] Lelito J, Żak P, Suchy JS, Krajewski W, Krawiec H, Greer AL, et al. *Mater Eng* 2010;3:703.
- [16] Lelito J, Żak P, Suchy J, Krajewski W, Krawiec H, Greer AL, et al. *World J Eng* 2010;7:1.
- [17] Rohatgi PK, Yarandi FM, Liu Y, Asthana R. *Mater Sci Eng A* 1991;147:L1.
- [18] Rohatgi PK, Ray S, Asthana R, Narendranath CS. *Mater Sci Eng A* 1993;162:163.
- [19] Ramesh CS, Ahmend RN, Mujeebu MA, Abdullah MZ. *Mater Design* 2009;30:1957.
- [20] Barmouz M, Givi MKB, Seyfi J. *Mater Char* 2011;62:108.
- [21] Luo A. *Scripta Metall Mater* 1994;31:1253.
- [22] Luo A. *Can Metall Quart* 1996;35:375.
- [23] Men H, Jiang B, Fan Z. *Acta Mater* 2010;58:6526.
- [24] Rauber C, Lohmüller A, Opel S, Singer RF. *Mater Sci Eng A* 2011;528:6313.
- [25] Bramfitt BL. *Metall Trans* 1971;6:1258.
- [26] Cai Y, Taplin D, Tan MJ, Zhou W. *Scripta Mater* 1999;41:967.
- [27] Cai Y, Tan MJ, Shen GJ, Su HQ. *Mater Sci Eng A* 2000;282:232.
- [28] Carslaw HS, Jaeger JC. *Conduction of heat in solids*. Oxford: Oxford Science Publishing; 1959. p. 230ff.
- [29] Tanzielli RA, Heckel RW. *Trans Metall Soc AIME* 1968;242:2313.
- [30] Maltais A, Dube D, Fiset M, Laroche G, Tugeon S. *Mater Char* 2004;52:103.
- [31] Maltais A, Fiset M, Dube D. *Microsc Microanal* 2005;11:694.
- [32] Cybo J, Jura S. *Funkcyjny opis struktur izometrycznych w metalografii ilościowej*. Gliwice: Wydawnictwo Politechniki Śląskiej; 1995 [in Polish].
- [33] Greer AL, Bunn AM, Tronche A, Evans PV, Bristow DJ. *Acta Mater* 2000;48:2823.
- [34] Fraś E, Wienczek K, Górny M, López H. *Mater Sci Technol* 2003;19:1653.
- [35] Tronche A, Greer AL. In: Peterson RD, editor. *Light Metals 2000*. Warrendale, PA: TMS; 2000. p. 827.
- [36] Quedstedt TE, Greer AL. *Acta Mater* 2004;52:3859.
- [37] Lu L, Dahle AK, StJohn DH. *Scripta Mater* 2006;54:2197.
- [38] Huang Y, Kainer KU, Hort N. *Scripta Mater* 2011;64:793.
- [39] Housh S, Mikucki B, Stevenson A. *Metals handbook*, vol. 2. Materials Park, OH: ASM International; 1990. p. 480.
- [40] Kurz W, Fisher DJ. *Fundamentals of solidification*. Zurich: Trans Tech Pub; 1992. p. 23.
- [41] Maxwell I, Hellawell A. *Acta Metall* 1975;23:229.
- [42] Hunt JD, Fan Z. In: Fan Z, Stone IC, editors. *Solidification science and technology*. Uxbridge: Brunel University Press; 2011. p. 59.
- [43] Built-in material database of MAGMASoft 4.2 software. Aachen, Germany; 2002.
- [44] Asthana R. *Key Eng Mater* 1998;151–152:1.